MULTI-MODAL 3D RECONSTRUCTION AND MEASUREMENTS OF ZEBRAFISH LARVAE AND ITS ORGANS USING AXIAL-VIEW MICROSCOPY

Y. Guo[1,†], R.C. van Wijk[2], E.H.J. Krekels[2], H.P. Spaink[3], P.H. van der Graaf[2,4] and F.J. Verbeek[1,†]

{1. Imaging and Bioinformatics Group, LIACS; 2. Division of Pharmacology, LACDR;
3. Division of Animal Sciences and Health, IBL}, Leiden University, The Netherlands.
4. Certara QSP, Canterbury, UK. † Email: {y.guo.3, f.j.verbeek}@liacs.leidenuniv.nl

ABSTRACT

In life sciences, light microscopy is used to study specimens. On the organism-level a bright-field representation present an overview for the whole shape of a specimen; the organ-level fluorescent staining representation supports in the interpretation of the detailed intrinsic structures. We present light microscopy axial-view imaging based on the Vertebrate Automated Screening Technology to acquire axial-view images for the organism and organs of zebrafish larvae. We obtain multi-modal 3D reconstruction using a profile-based method, from which we can derive the 3D measurements of volume and surface area. In this method, we employ a microscope camera calibration using voxel residual volume maximization algorithm. We intuitively align and fuse the obtained multi-models. Experimental results show natural visualization both for the whole organism and organ of zebrafish larvae; subsequently accurate 3D measurements are obtained. This method is very suitable for high-throughput research in which knowledge on size and shape is relevant to the understanding for development, effects of compounds or drugs.

***Index Terms*—** Multi-modal 3D reconstruction, 3D measurements, zebrafish and organ, axial-view microscopy

1. INTRODUCTION AND RELATED WORK

In modern life-sciences research, e.g. developmental biology, (patho)physiology, toxicology, and pharmacology, light microscopy is commonly used to produce 2D color representations of biological phenomena. Zebrafish is a popular vertebrate model organism in biomedical research because of its many advantages, among which is optical transparency at early stages [1, 2]. The organs of the transparent larvae can be studied *in vivo* through microscopy. Transgenic lines are available that express a fluorescent reporter gene in specific organs, tissues, or cell types [3]. In this way, organ development of the genetically engineered zebrafish can be visualized and monitored over time by fluorescence microscopy. This makes the zebrafish very suitable for large scale screening experiments using light microscopy. For the screening of large libraries of compounds for organ toxicity, like hepatotoxicity [4], quantitative endpoints like organ size or growth retardation are required. In order to accurately evaluate the shape and size of an organ like the liver, 3D modelling of both the liver and the whole organism are required. Compared with 2D imaging, 3D measurements, e.g. size, volume and surface area, are more reliable. The organism-level imaging is an overview of the shape of the object, serving as shape reference to normalize the 3D measurements of liver into unit metrics. Our aim is to develop a method for 3D reconstruction and measurements of zebrafish larvae and its organs using axial-view microscopy.

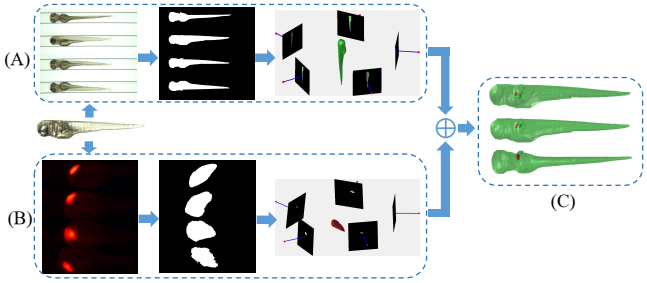

Fig. 1: A schema of the proposed method. One zebrafish larva presents in the two imaging pipelines. (A) The organism-level 3D reconstruction. (B) The organ-level 3D reconstruction. (C) The multi-modal 3D reconstruction fusion and visualization. In (A) and (B), the first columns show the original axial-view images; the second columns illustrate the 2D binary shapes; the third columns denote the camera system calibration and profile-based 3D reconstruction.

In stereo vision, a 3D scene can be recovered by matching correlated multi-view images [5]. This is implemented by pixel-level searching [6] or salient point detection and matching [7]. However, these methods are challenged for our typical application at hand, the zebrafish. Here, partial transparency of the zebrafish complicates straightforward application of these methods as it is difficult to match the implicit surface points on the object. Based on the concept of visual hull [8], the space carving algorithm reconstructs the 3D shape from a range of 2D binary shapes [9], which is also re-

ferred to as the silhouette-based 3D reconstruction [10, 11]. In a sample population of zebrafish a rather large color variation exists; this holds both for bright-field and fluorescence. Therefore, we propose to use 2D binary representations. Accordingly, we have developed the profile-based 3D zebrafish reconstruction method based on a series of 2D axial-view shapes of the object, obtaining a precise 3D representation and accurate 3D measurements in various larval stages [12].

For this work, we have implemented light microscopy axial-view imaging modality based on the Vertebrate Automated Screening Technology (VAST BioImager) [13, 14]. Using the axial-view images acquired from this multi-modal imaging modality, we propose a multi-modal 3D reconstruction method as framed in Fig. 1. A zebrafish larva with fluorescent marker expressed in the liver is captured in two imaging modes. The VAST camera enables the organism-level imaging and a microscope camera facilitates the organ-level imaging. From the axial-view images, 2D binary shapes are obtained through modern segmentation algorithms [15, 16]. We estimate the camera projection geometry for the two camera systems using the voxel residual volume maximization algorithm. We produce the multi-modal 3D reconstruction for the organism (zebrafish) and organ (liver) using the profile-based 3D reconstruction method; we use heuristics to fuse the two models acquired from different imaging modalities. From the obtained 3D models, 3D measurements, e.g. volume and surface area, are derived.

2. OUR APPROACH

In this section, we present multi-modal microscopy axial-view imaging. A dataset containing the zebrafish on both organism- and organ-level imaging is obtained. We introduce the microscope camera calibration and elaborate profile-based 3D reconstruction. We present an interactive method to align and fuse the multi-modal 3D reconstruction.

2.1. Light microscopy axial-view imaging

For VAST imaging, zebrafish are positioned along their longitudinal axis. This facilitates easy manipulation of the specimen and the most important features of the specimen can be observed well from the axial-view. The VAST-BioImager is developed for zebrafish high-throughput applications [17]. We use this device for our axial-view imaging and thereby generate new functionality of the device. In Fig. 2 , a schematic representation is shown depicting the imaging architecture. The positioning module of the VAST BioImager consists of a capillary and a pair of stepper motors facilitating the rotation of the specimen. A standard CCD camera referred to as the VAST camera #1 is mounted with the device and used to detect the location and orientation of the specimen. We use the VAST camera #1 to acquire the bright-field axial-view images on the organism-level. The VAST-unit

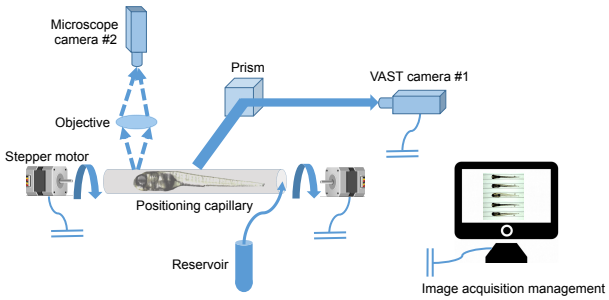

Fig. 2: An architecture for light microscopy axial-view imaging. The VAST-BioImager delivers a specimen from its reservoir into a capillary. A set of stepper motors hold and manipulate the capillary so that it can rotate in a full revolution; this is synchronised with acquisition so that axial-view images of the specimen can be obtained. The VAST camera #1 detects the presence of a specimen and generates the axial-view images capturing the whole organism in bright-field. The microscope camera #2 captures the organ-level axial-view images in fluorescence.

is mounted on a microscope. We use the microscope camera #2 equipped with a 4×/0.12NA objective to acquire the fluorescent images for the liver on organ-level. This imaging technique is applied to collect a dataset of 7 zebrafish samples, staged as three days post fertilization (3 dpf)[1]. We evenly sampled 25 axial-views for each zebrafish in both channels in a full revolution. This means the step between adjacent views is approximately 14.4^o (due to mechanical drift this is not precise).

2.2. Profile-based 3D reconstruction

Given a range of axial-view images $\mathbf{I}$, we first obtain the 2D profiles $\mathbf{S}$ for the object (zebrafish and liver) from image segmentation. We interpret the 3D space in discrete voxel units. Given a voxel centred at a 3D point $\mathbf{X} \in \mathcal{R}^3$, we can find its pixel location $\mathbf{x} \in \mathcal{R}^2$ in a 2D profile according to the camera projection model $\mathbf{x} = \mathbf{PX}$. The profile-based 3D reconstruction projects all the voxels onto all the 2D profiles. According to the visibility of a voxel w.r.t. the profiles, we assign a confidence score to that voxel. The confidence score is actually the total number of the profiles which can cover the pixel location of that voxel. The 3D reconstruction is accomplished by extracting the voxels given a threshold for a confidence score (usually taken as the total number of the axial-views). One can also estimate an enclosed 3D surface from the voxels. For more details of the profile-based 3D reconstruction, we refer to our previous work [12, 18].

[1]A zebrafish transgenic line Tg(lfabp:dsRed; elaA:EGFP) with 2 fluorescent colors for liver and pancreas (2CLIP) is used. The eggs were kept in 60 $\mu g/mL$ Instant Ocean Sea Salts (Sera Marin, Heinsberg Germany) in demineralized water and treated with 0.003% 1-phenyl-2-thiourea (PTU, Sigma-Aldrich, Zwijndrecht The Netherlands) to prevent pigmentation.

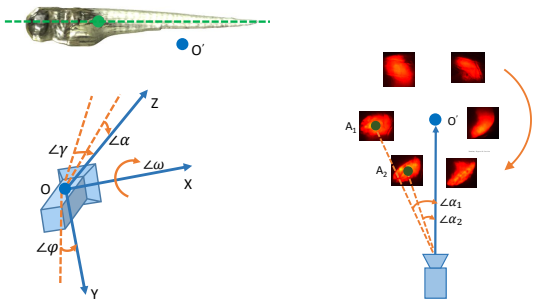

(a) (b)

Fig. 3: (a) The VAST camera pose is modelled as the 3D transformation from the camera center O to the object center (green circle). The green line denotes the profile-axis along which the object revolves. $\angle\omega$, $\angle\varphi$ and $\angle\gamma$ represents the 3D rotation angles of the camera along the X, Y and Z directions, respectively. $\angle\alpha$ is modelled as the "translation angle". (b) The center of the zebrafish liver is not aligned with the zebrafish center which results in its rotation and revolution w.r.t the zebrafish center, such that the "translate angle" $\angle\alpha$ of the microscope camera is specified for each view.

2.3. Light microscope camera system calibration

For a good profile-based 3D reconstruction, we need an accurate camera projection model which can be obtained from a camera calibration. We decompose the camera projection matrix as $\mathbf{P} = \mathbf{K}\,\mathbf{R}\,[\,\mathbf{I}\mid\mathbf{T}\,]$. The $\mathbf{K}$ denotes the camera intrinsic configuration defined as:

$$\mathbf{K} = \begin{bmatrix} f*k_x & 0 & c_x \\ 0 & f*k_y & c_y \\ 0 & 0 & 1 \end{bmatrix}, \qquad (1)$$

where f is the camera focal length; (k_x, k_y) denotes the scaling factor and (c_x, c_y) represents the image center. In the decomposition of the camera projection model, the $\mathbf{R}_{3\times3}$ and $\mathbf{T}_{3\times1}$ are the 3D rotation and translation from the camera center to the object center, which are also referred to as the camera motion. In practice, the camera remains static and only the specimen rotates. For visualization purposes, we arranged the camera as moving around the object as shown in Fig. 1.

In Fig. 3(a), we show the VAST camera motion w.r.t. the zebrafish center. The zebrafish revolves along a fixed profile-axis which is aligned with the object center, such that the VAST cameras share the rotation angles φ and γ and the translation angle α [19]. The camera rotation angle along the X-axis is specified for each view. So, the whole camera configuration is structured as $\psi = [f, k_x, k_y, c_x, c_y, \alpha, \varphi, \gamma, \omega_{1:N}]$, where N is the number of the axial-views. For the microscope cameras, the rotation center of the zebrafish liver is not aligned with its own center as shown in Fig. 3(b), so the translation angle should be specified for each view. We improve the parameterization for microscope camera configuration as $\psi = [f, k_x, k_y, c_x, c_y, \alpha_{1:N}, \varphi, \gamma, \omega_{1:N}]$. The method of voxel residual volume maximization (VRV) is used to estimate accurate camera configuration. The objective is defined as $\mathcal{L}(\psi) = |\mathcal{X}^*|$, where $\mathcal{X}^* = \{\mathbf{X} \mid \mathcal{S}(\mathbf{P}(\psi)\mathbf{X}) \neq 0, \mathbf{X} \in \mathcal{X}\}$ and $|\mathcal{X}^*|$ are the voxel residual and the volume. The objective maximization is implemented by Nelder-Mead simplex method [20].

2.4. Multi-modal 3D reconstruction alignment and fusion

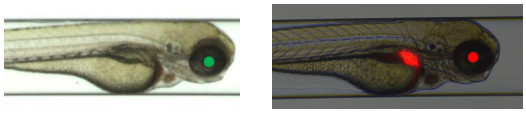

Fig. 4: The alignment of the multi-modal 3D reconstruction is implemented according to the iris center of the zebrafish. On the left-side is a bright-field image of organism-level imaging. We crop this image to fit the space. On the right-side is a bright-field image overlaid with a fluorescent image of organ-level imaging.

The 3D models are obtained from different imaging modes. So, we need to align the resulting multi-modal 3D reconstruction as part of the fusion operation. During the organ-level imaging, we acquired bright-field images in register with the fluorescent images. These images only partially depict the object but provide a good reference for alignment. We have obtained the camera poses for both models from camera calibration. So, we choose the same axial-view for the zebrafish and localize the iris center as shown in Fig. 4. We use the organ-level 3D model as a template. The organism-level 3D model is scaled, rotated and shifted to align with the former according to the camera pose and the position of the iris center. Finally, we map the multi-models into the same space to obtain the fusion result.

3. EXPERIMENTS

In this section, we apply our method on the zebrafish dataset for performance evaluation. We first visualize some examples of the multi-modal 3D reconstruction in section 3.1, and subsequently report on the 3D measurements of volume and surface area for the zebrafish larvae and its liver in section 3.2.

3.1. Results visualization

From our dataset, we select three examples for visualization as shown in Fig. 5[2]. Two typical axial-views are shown, i.e. lateral and dorsal and each example is separated by blue lines. The first column shows the original organ-level fluorescent images. Those images depict the natural shape of the zebrafish liver. One can observe a variation in image quality

[2]An animated visualization of the results can be found at `http://bio-imaging.liacs.nl/galleries/VAST-3Dorgan/`

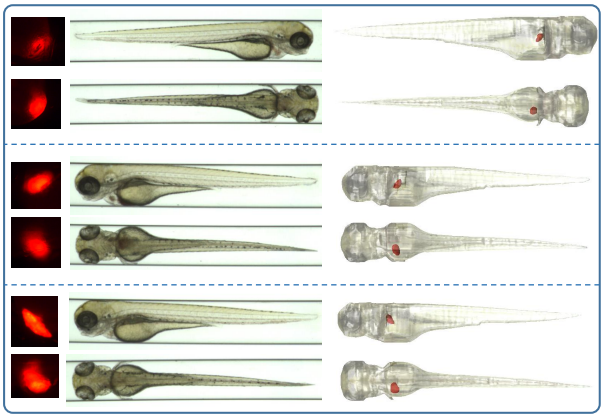

Fig. 5: Multi-modal 3D reconstruction visualization. We selected three examples from our dataset and for each example we visualize two typical views (lateral and dorsal). The first column represents fluorescent liver images. The middle column is the zebrafish image in bright-field. The last column visualizes the fusion of the multi-modal 3D reconstruction. One can zoom in for a better observation.

Table 1: 3D measurements of the 3D reconstructed models for the zebrafish (ZF) and its liver (Liver)

	Volume		Surface area	
	ZF	Liver	ZF	Liver
	$(\times 10^8 \mu m^3)$	$(\times 10^5 \mu m^3)$	$(\times 10^6 \mu m^2)$	$(\times 10^4 \mu m^2)$
#1	2.74	7.70	3.33	4.67
#2	2.59	5.38	3.24	3.61
#3	2.50	8.01	3.13	4.91
#4	2.91	9.06	3.44	5.20
#5	2.67	11.60	3.31	6.07
#6	2.80	15.15	3.47	6.89
#7	2.80	6.55	3.41	4.28

from the different examples. This is caused by strength of the fluorescent marker. The middle column shows the organism-level bright-field images. The zebrafish are partially transparent but retains explicit contours for the shape. The last column visualizes the fusion of the 3D models. For a natural appearance, we map the texture from the zebrafish to the 3D model. One can clearly observe the shape of both the zebrafish and its liver. The visual and spatial discernibility of the models are emphasized from the multi-modal fusion. It is interesting that, although the liver is not completely visible in a all views (the first view of the first example), our method still recovers a good 3D shape by imposing a threshold to the confidence score to estimate a 3D model allowing a range of errors.

3.2. 3D measurements for multi-modal 3D reconstruction

From the multi-modal 3D reconstruction, we derive 3D measurements, i.e. volume and surface area. The volume is obtained by the integration over all the voxels included in the object. A set of surface points is generated from the voxels by the marching cubes algorithm [21], from which a triangulated mesh can be produced. The obtained 3D surface is further refined [22]. Subsequently, the surface area is obtained by the integration of all the facets in the triangulated mesh using Heron's formula [23]. In Table 1 we report on the computed 3D measurements of volume and surface area for both zebrafish and its liver.

In previous work [12], we have reported accurate 3D measurements for the 3 dpf zebrafish, from which we obtained the volume statistics as 2.53 ± 0.11 $(\times 10^8 \mu m^3)$ and the surface area as 3.20 ± 0.15 $(\times 10^6 \mu m^2)$. In this experiment, the statistics of the 3D measurements for the zebrafish are 2.72 ± 0.14 $(\times 10^8 \mu m^3)$ for the volume and 3.33 ± 0.12 $(\times 10^6 \mu m^2)$ for the surface area. The phenomenon that the specimens in this experiment are larger compared to our reference set is due to the fact that we did not accurately time the development for this experiment. We also computed the statistics of the 3D measurements for the liver as 9.06 ± 3.33 $(\times 10^5 \mu m^3)$ for the volume and 5.09 ± 1.10 $(\times 10^4 \mu m^2)$ for the surface area. The shape variation of the zebrafish liver is large for different individuals, but we can observe that a larger zebrafish tends to have a larger liver [24].

We implemented our method using Matlab programming on a desktop with an Intel i7 CPU and a 16G RAM. We evaluate the efficiency as runtime for the 3D reconstruction of the zebrafish and its liver separately as $22.0 \pm 0.4(s)$ $26.3 \pm 1.3(s)$. The results of this experiment can be directly used for establishing physiological values of a healthy liver of a 3 dpf zebrafish. This method can be more generically used to assess all observable effects of any compound on the shape and size of an organ.

4. CONCLUSIONS AND FUTURE WORK

In this paper, we have presented a method for multi-modal 3D reconstruction and fusion on both organism- and organ-level through light microscopy axial-view imaging. We have implemented the imaging architecture using the VAST BioImager and applied our method to zebrafish larvae. Within the reconstructed 3D models, we observe an overview shape for the object on the organism-level and the detailed structure on the organ-level. The former provides a good shape reference to normalize and evaluate the organ development in phenotypical research. The experimental results show natural visualization of the multi-modal fusion images. Additionally, accurate 3D measurements are obtained, which can be directly used for the evaluation of the biological system with compound screening. This method can be further developed to determine size and shape of other fluorescently labelled organs and objects, like pathogens or tumour cells. In order to further improve this work, a larger sample size of our subjects should be considered to get better statistics for the 3D measurements. High-throughput imaging would be a good approach for this.

5. REFERENCES

[1] R.C. van Wijk, E.H.J. Krekels, T. Hankemeier, H.P. Spaink, and P.H. van der Graaf, "Systems pharmacology of hepatic metabolism in zebrafish larvae," *submitted*, 2017.

[2] A.J. Rennekamp and R.T. Peterson, "15 years of zebrafish chemical screening," *Curr. Opin. Chem. Biol.*, vol. 24, pp. 58–70, 2015.

[3] E. Moro et al., "Generation and application of signaling pathway reporter lines in zebrafish," *Mol. Genet. Genomics*, vol. 288, pp. 231–242, 2013.

[4] P. McGrath and C. Li, "Zebrafish: a predictive model for assessing drug-induced toxicity," *Drug Discov. Today*, vol. 13, pp. 394–401, 2008.

[5] R. Hartley and A. Zisserman, *Multiple view geometry in computer vision*, Cambridge university press, 2003.

[6] K. Yoon and I.S. Kweon, "Adaptive support-weight approach for correspondence search," *TPAMI*, , no. 4, pp. 650–656, 2006.

[7] M. Brown and D.G. Lowe, "Automatic panoramic image stitching using invariant features," *IJCV*, vol. 74, no. 1, pp. 59–73, 2007.

[8] A. Laurentini, "The visual hull concept for silhouette-based image understanding," *TPAMI*, vol. 16, no. 2, pp. 150–162, 1994.

[9] Y. Furukawa and J. Ponce, "Carved visual hulls for image-based modeling," *IJCV*, vol. 81, no. 1, pp. 53–67, 2009.

[10] D. Cremers and K. Kolev, "Multiview stereo and silhouette consistency via convex functionals over convex domains," *TPAMI*, vol. 33, no. 6, pp. 1161–1174, 2011.

[11] K. Kolev, T. Brox, and D. Cremers, "Fast joint estimation of silhouettes and dense 3d geometry from multiple images," *TPAMI*, vol. 34, no. 3, pp. 493–505, 2012.

[12] Y. Guo, W.J. Veneman, H.P. Herman, and F.J. Verbeek, "Three-dimensional reconstruction and measurements of zebrafish larvae from high-throughput axial-view *in vivo* imaging," *Biomed. Opt. Express.*, vol. 8, no. 5, pp. 2611–2634.

[13] C. Pardo-Martin, T. Chang, B.K. Koo, C.L. Gilleland, S.C. Wasserman, and M.F. Yanik, "High-throughput in vivo vertebrate screening," *Nat. methods*, vol. 7, no. 8, pp. 634–636, 2010.

[14] R. Pulak, "Tools for automating the imaging of zebrafish larvae," *Methods*, vol. 96, pp. 118–126, 2016.

[15] V. Caselles, R. Kimmel, and G. Sapiro, "Geodesic active contours," *IJCV*, vol. 22, no. 1, pp. 61–79, 1997.

[16] D. Comaniciu and P. Meer, "Mean shift: A robust approach toward feature space analysis," *TPAMI*, vol. 24, no. 5, pp. 603–619, 2002.

[17] W.J. Veneman, R. Marín-Juez, J. de Sonneville, A. Ordas, S. Jong-Raadsen, A.H. Meijer, and H.P. Spaink, "Establishment and optimization of a high throughput setup to study staphylococcus epidermidis and mycobacterium marinum infection as a model for drug discovery," *J. Vis. Exp.*, , no. 88, 2014.

[18] Y. Guo, W.J. Veneman, H.P. Spaink, and F.J. Verbeek, "Silhouette-based 3d model for zebrafish high-throughput imaging," in *IPTA'15*. IEEE, 2015, pp. 403–408.

[19] C. Hernández, F. Schmitt, and R. Cipolla, "Silhouette coherence for camera calibration under circular motion," *TPAMI*, vol. 29, no. 2, pp. 343–349, 2007.

[20] J.C. Lagarias, J.A. Reeds, M.H. Wright, and P.E. Wright, "Convergence properties of the nelder–mead simplex method in low dimensions," *SIAM J. Optim.*, vol. 9, no. 1, pp. 112–147, 1998.

[21] W.E. Lorensen and H.E. Cline, "Marching cubes: A high resolution 3d surface construction algorithm," in *ACM Siggraph Computer Graphics*. ACM, 1987, vol. 21, pp. 163–169.

[22] M. Desbrun, M. Meyer, P. Schröder, and A.H. Barr, "Implicit fairing of irregular meshes using diffusion and curvature flow," in *ACM Conference on Computer Graphics and Interactive Techniques*. ACM Press/Addison-Wesley Publishing Co., 1999, pp. 317–324.

[23] L. Cao and F.J. Verbeek, "Evaluation of algorithms for point cloud surface reconstruction through the analysis of shape parameters," in *J. Electron. Imaging*. International Society for Optics and Photonics, 2012, pp. 82900G–82900G.

[24] H.A. Field, E.A. Ober, T. Roeser, and D.Y.R. Stainier, "Formation of the digestive system in zebrafish. i. liver morphogenesis," *Deve. Biol.*, vol. 253, no. 2, pp. 279–290, 2003.